The Role of Giant and Ultragiant Nuclei in the Formation of Early Radar Echoes in Warm Cumulus Clouds

ALAN M. BLYTH* AND SONIA G. LASHER-TRAPP

Department of Physics and Geophysical Research Center, New Mexico Institute of Mining and Technology, Socorro, New Mexico

WILLIAM A. COOPER, CHARLES A. KNIGHT, AND JOHN LATHAM

National Center for Atmospheric Research,+ Boulder, Colorado

(Manuscript received 20 August 2001, in final form 20 May 2003)

ABSTRACT

Observations of the formation of the first radar echoes in small cumulus clouds are compared with results of a stochastic coalescence model run in the framework of a closed parcel. The observations were made with an instrumented aircraft and a high-powered dual-wavelength radar during the Small Cumulus Microphysics Study (SCMS) in Florida. The principal conclusion is that coalescence growth on giant and ultragiant nuclei may be sufficient to explain observations.

The concentration of cloud droplets varied from under 300 cm^{-3} when surface winds were from the ocean, to over 1000 cm^{-3} when the wind direction was from the mainland. Although there is a slight tendency for the altitude of the first 0-dBZ echo to be lower on average in maritime than in continental clouds there were several cases where it was higher. The model results suggest that the lack of correlation is consistent with drops forming on giant and ultragiant nuclei. The first 0-dBZ echo was observed to form at higher altitudes in clouds with stronger updrafts.

1. Introduction

A significant fraction of precipitation that falls in the Tropics is warm rain formed by the coalescence of cloud droplets. Despite 50 years of research on this topic, we still do not possess a quantitative understanding of the production of warm rain. It is commonly stated that condensation and ''ordinary'' collision and coalescence theory cannot produce rain in an observed time to rain of 20 min (e.g., Rogers and Yau 1989). Several ideas have been proposed to speed up the process. However, cloud models are not yet able to simultaneously reproduce the 3D dynamics of the cloud and the drop size distribution at each grid point at appropriate spatial and temporal resolutions, and the observations are not good enough to compare with the models in any case. It is notoriously difficult to measure the drop size distribution in the key regions of cloud. One approach is to test the known hypotheses: for example, short circuiting due to the presence of giant and ultragiant nuclei (UGN[1]), enhanced condensational growth due to mixing, or enhanced collision efficiencies due to turbulent capture of drops.

Pinsky et al. (1999, 2000) suggested in a theoretical study that turbulence significantly increases the collision efficiency particularly for small cloud droplets with radii below 10–15 μm. Pinsky et al. (2001) further suggested that the enhancement increases with height because of the increase in turbulence intensity and the increase in the relative velocities between droplets. Laboratory measurements of coalescence efficiencies are normally performed in still air, so the effects of turbulence are not known.

Hu et al. (1998) studied the effects of van der Waals forces on enhancing collision and coalescence and found that including these forces in the model increases the rate of droplet collisions for small droplets and narrow distributions, but the effect decreases as the droplets increase in size. There was no effect on maritime clouds.

Johnson (1982), in a seminal paper employing a sto-

* Current affiliation: Institute for Atmospheric Science, School of the Environment, University of Leeds, Leeds, United Kingdom.

+ NCAR is sponsored by the National Science Foundation.

Corresponding author address: Alan M. Blyth, Institute for Atmospheric Science, School of the Environment, University of Leeds, Leeds LS2 9JT, United Kingdom.
E-mail: blyth@env.leeds.ac.uk

[1] Ultragiant aerosols (UGAs) and ultragiant nuclei are often used to describe the same particles. Which term to use depends on the context of the study. In this paper, the context is entirely the influence of particles on cloud drop populations, so UGN is appropriate. Giant and ultragiant particles are defined to have radii of $1 < r \leq 10$ μm and $r > 10$ μm, respectively.

chastic collision and coalescence model, examined the influence of UGN on the formation of warm rain and concluded that ''naturally occurring giant and ultra-giant aerosol particles can play an important role in precipitation initiation.'' A number of other modeling studies (e.g., Ochs and Semonin 1979) have shown that these largest aerosol particles play a significant role in the initial development of warm rain. Further support for this contention has been supplied by Beard and Ochs (1993) and Szumowski et al. (1999). Caylor and Illingworth (1987) found that radar observations of the early development of differential reflectivity Z_{DR} and reflectivity could be explained by using UGN. Lasher-Trapp et al. (2001) calculated drop growth on UGN by continuous collection in a high-resolution, three-dimensional simulated cloud, and they found that the altitudes and magnitudes of the observed first echoes could be explained by UGN. Laird et al. (2000) presented size distributions from the 260X probe; which suggested that giant and ultragiant nuclei were present in clear air. They concluded that their analysis provided strong evidence that raindrop embryos form on ultragiant nuclei. However, Lasher-Trapp et al. (2002) concluded that these distributions were mainly caused by noise.

Giant aerosols were first reported by Woodcock (1953), who found that size distributions measured over the sea near Hawaii were very sensitive to wind speed. Mészáros and Vissy (1974), Exton et al. (1985), de Leeuw (1986), and O'Dowd et al. (1997) have presented further data supporting Woodcock's observations.

In this paper, we examine the role of UGN in the development of the early radar echoes. We present observations of the early stages of several small cumulus clouds made with an aircraft and a high-sensitivity radar during the Small Cumulus Microphysics Study (SCMS), conducted in the summer of 1995 near Cape Canaveral, Florida, and examine if the early radar echoes in single-ascent clouds can be reproduced in a simple parcel model with collision and coalescence calculations that include giant and ultragiant nuclei. Observations from several clouds are presented and four of them are compared with results from a stochastic coalescence model.

Section 2 of the paper describes the measurements made during SCMS. Section 3 discusses the condensation and stochastic coalescence model and the parcel model framework. Radar and aircraft observations of more than 20 clouds are presented in section 4 and observations and model runs for four of the clouds are presented in section 5. The conclusions and discussion are in section 6.

Times quoted are in universal time coordinated (UTC) and all altitudes are above mean sea level (MSL), unless otherwise stated.

2. Details of the study

The Small Cumulus Microphysics Study was conducted in Florida near Cape Canaveral from 7 July to 13 August 1995. The experiment was designed to examine whether the initiation of warm rain could be explained simply by condensation and coalescence growth commencing on the nuclei that exist below cloud base, or if an additional process is required, such as enhanced growth of a few of the larger cloud drops due to entrainment and mixing. SCMS was the first field experiment focusing on the early development of warm clouds that utilized a radar [National Center for Atmospheric Research (NCAR) CP-2] that was sufficiently sensitive to detect signals from clouds in which coalescence had not yet started.

The primary observations were made with the NCAR CP-2 dual-wavelength radar (with wavelengths of $\lambda_X = 3$ cm, and $\lambda_S = 10$ cm for the X and S bands, respectively). The radar was sensitive to about -20 dBZ in both wavelengths, so clouds could be detected during the condensation phase (Knight and Miller 1993, 1998). The clouds were generally within the 20-km range of the radar, range–height indicator (RHI) scans were made every 1°–1.5°, and a cloud was completely scanned approximately every 2 min. The RHI with the maximum echo in the set of scans is used in time sequences in this paper. This was usually in the center of the cloud. Three aircraft participated in the study: the NCAR C-130, the University of Wyoming King Air, and the Météo France Merlin. Only the NCAR C-130 data are discussed in this paper. It was equipped with up-to-date microphysical instruments; measurements presented herein are primarily from the forward scattering spectrometer probe (FSSP) and 260X probes (e.g., Dye and Baumgardner 1984; Baumgardner et al. 1985; Baumgardner and Spowart 1990; Baumgardner and Korolev 1997). The FSSP and 260X were calibrated to measure droplets with sizes ranging between 0.5–50.5 μm and 17 μm–1.088 mm, respectively. The C-130 flew long flight legs at low levels each day, before the clouds were penetrated, to characterize the aerosol and cloud condensation nuclei (CCN) of the environment. We refer the reader to Hudson and Yum (2001) for a discussion of the CCN. It was anticipated that the 260X would provide estimates of the concentrations of the largest particles when averaged over these flight legs in the clear air.

Although the 260X did record counts in the clear air (Laird et al. 2000), it is unlikely that they represent real particles; it is now suspected that noise caused spurious counts (Lasher-Trapp et al. 2002). Upper limits on UGN concentrations derived from the few 2DC counts (Lasher-Trapp et al. 2002) suggest total concentrations of about 10 m^{-3}. The spatial and temporal variability of these concentrations during SCMS is unknown.

3. The model

We use the condensation and stochastic coalescence model discussed by Cooper et al. (1997) in a closed parcel framework and compare the results with the air-

craft and radar observations made in the clouds discussed in section 5. The model was run in a closed parcel with adiabatic liquid water content for a single ascent using the observed cloud base.

Although the parcel model is a useful tool for examining detailed microphysical processes in a simple dynamics framework, comparing the model results to measurements is not entirely straightforward. First and foremost, the assumption must be made that the simple dynamic framework is adequately realistic. Here, this means assuming that the development of the first 0-dB*Z* echo did form in a single, simple ascent from cloud base, starting from the aerosol. Since the height of the 0-dB*Z* first echo above cloud base is used as a proxy for the time it takes to form the echo, it is also necessary to assume that fall velocities of the hydrometeors responsible for the first echo are negligible, for this purpose. Recent polarimetric radar results suggest that drop sizes responsible even for 0 dB*Z* can be large (e.g., Knight et al. 2002). However, in view of the facts that for the four clouds studied in detail in this paper, the first 0-dB*Z* echo is near cloud top and that the cloud top itself is rising, the hydrometeors that constitute it must have come from below.

In particular, fitting the model to individual cases requires consideration of the updraft speed, the cloud liquid water content, and the size distribution of the nuclei at cloud base.

The model updraft was adjusted to match the radar-observed cloud-top ascent rate of the cloud during the initial ascent of the cloud. The ascent rate in the lowest 1 km is difficult to determine from measurements, so a value of 2 m s^{-1} is used unless backward projections from the radar data suggested a different value. The value of 2 m s^{-1} is consistent with what was measured with the aircraft. Sensitivity studies conducted for initial ascent rates of 2 and 3 m s^{-1} are discussed in section 5a(2).

Lasher-Trapp et al. (2001) used trajectories of packets of UGN calculated within the 3D wind and cloud water field produced by a sophisticated cloud model (Carpenter et al. 1998) and concluded that the 0-dB*Z* echo in a cloud that formed on 22 July 1995 could have been produced by the growth of UGN particles that made a single straight ascent from cloud base in an approximately adiabatic cloud. This result is consistent with the radar observations from SCMS showing that the maximum echoes form in the upper center of the cloud and not, for example, along the edges as might be expected if large drops continued growing as they are transported into the downdrafts.

The cloud liquid water content in the model is the undiluted value of an adiabatic process. So the calculations provide an upper limit for growth with ordinary coalescence. Further discussion of this model limitation will be given on a case-by-case basis.

The appropriate values of *C* and *k* that define the CCN spectrum for each day are used for the small end of the input CCN distribution (J. Hudson personal communication, 2001). These are 2000, 1000, 600, and 450 cm^{-3} for 20 and 24 July and 10 and 4 August, respectively. Values used for *k* are 0.73 and 0.60 for continental (July) and maritime (August) cases, respectively. Since there was no reliable measurement of giant or ultragiant nuclei, two distributions are used: a distribution that is consistent with the one based on the 2DC data produced by Lasher-Trapp et al. (2002) (the ''standard'' case) and one with small concentrations of giant and ultragiant nuclei (henceforth called the ''reduced-ugn'' case). Figure 1 shows the two distributions for 100% relative humidity and typical values of *C* and *k.*

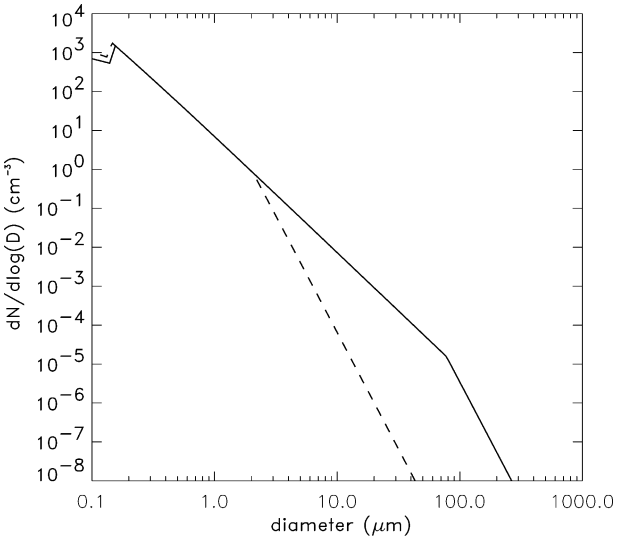

FIG. 1. Initial size distributions at 100% relative humidity used for the model runs. The solid line is the standard case and the dashed line is the reduced-ugn case.

4. General features of the clouds

The cumulus clouds studied during SCMS typically had bases at pressure of 940 mb (about 500 m MSL) and a temperature of 23°C. We concentrate in this paper on small, early clouds with typical widths between 1 and 2 km and depths between 2 and 4 km. The altitude of the freezing level during the project was typically 5 km.

The wind direction on 19–24 July and 11–13 August had a significant component from the Florida mainland and as a result, the clouds were ''continental'' with a typical maximum concentration of cloud droplets of 800 cm^{-3} or more[2] (Hudson and Yum 2001). The clouds that formed on 28 July–4 August when the wind was from the Atlantic Ocean contained significantly fewer drop-

[2] The maximum concentrations of cloud droplets reported here are likely to be lower than the actual maxima because of coincidence errors (Cooper 1988) and because the aircraft did not sample adiabatic regions in every cloud.

TABLE 1. Key features of clouds that were tracked by the radar during SCMS. Columns 2–7 are, respectively, the observation times, the maximum number concentration of cloud droplets, the maximum altitude of the radar top, the maximum reflectivity observed in the cloud, the altitude range of the first appearance of the 0-dB*Z* echo, the average ascent rate of the radar top, and the average rate of increase of relectivity during the ascent stage. The clouds on 20 and 24 Jul, and 4 and 10 Aug are shown in Figs. 4, 5, 13, and 9. The ascent rate for the 5 Aug case applied to the initial ascent of the clouds to about 2.7 km. Thereafter the clouds ascended very slowly or in spurts as new thermals came through.

Date (1995)	Times (UTC)	N_{max} (cm^{-3})	z_{max} (km)	Max reflectivity (dB*Z*)	Altitude 0 dB*Z* (km)	Ascent rate ($m\ s^{-1}$)	Reflectivity rate (dB*Z* min^{-1})
18 Jul	1609–1629	600	3	15	2.0–2.1*	2.3	1.4
18 Jul	1619–1636		2.9	10	1.7–2.4*	2.1	1.5
20 Jul	1546–1553	1000	4	0	2.6–3.2	3.8	1.6
22 Jul	1512–1532	600	5	10	3.2–3.5	5.1	2.1
24 Jul	1629–1634	800	4	0	2.9–4.1	8.1	3.3
26 Jul	1546–1604	700	4.2	15	2.8–3.8	3.4	1.7
27 Jul	1551–1600	300	4.1	15	2.7–2.8	3.3	2.2
4 Aug	1458–1508	300	4	15	2.8–3.8	3.5	2.1
4 Aug	1500–1517		4.5	20	3.2–3.7	4.3	1.5
4 Aug	1502–1522		4.5	35	2.7–2.9	3.7	1.8
4 Aug	1509–1531		5.5**	55	2.5–3.5	3.7	2.7
4 Aug	1544–1600		3.5	5	2.5–3.0	2.6	0.9
5 Aug	1217–1245	300	4	45	2.0–2.3	2.2	3.9
5 Aug	1247–1307		3.5	15	2.2–2.4	3.0	1.8
5 Aug	1247–1319		3.5	35	2.0	1.8	1.5
5 Aug	1412–1428		3.25	15	2.5–2.7	1.8	1.7
10 Aug	1458–1507	530	4.5	30	2.1–2.3	3.6	4.7
10 Aug	1507–1522		3	5	2.0	2.4	1.4
10 Aug	1553–1618		4	30	2.5	2.2	2.8
10 Aug	1557–1618		5.5**	55	2.3–2.9	3.2	3.9
10 Aug	1647–1708		5.6	55	2.5–2.9	2.8	5.0
10 Aug	1719–1736		3.8	15	2.6–3.2	1.5	2.1

* Reflectivity developed to 0 dB*Z* after the cloud had reached its maximum top.
** Scan was not quite high enough to measure the very top of the cloud.

lets than the continental clouds. The wind direction on 31 July had the greatest easterly component of any day in the project and the clouds which formed contained the lowest concentration of cloud droplets: a maximum of 225 cm^{-3} was measured. The maximum concentration of cloud droplets on 28 July and 4 August was about 400 and 300 cm^{-3}, respectively, suggesting that the air mass was somewhat continental on both days. The wind was parallel to the shoreline on several days including 10 August when the maximum number of cloud droplets measured was 530 cm^{-3}. Further details of the variation of the concentration of CCN and cloud droplets as a function of wind direction are given by Hudson and Yum (2001).

Table 1 gives information derived from radar and aircraft data for 22 clouds that were tracked by the radar. These cases have the most complete histories. Although the radar sampled many clouds, only a small subset were tracked completely enough for inclusion in our analysis. It was not possible to track clouds on 31 July, for example, because of the high wind speeds preceding Hurricane Erin. Table 1 shows the variation from day to day of the project, as well as the variation on some individual days. In most of the cases listed, the radar top ascended continuously to the maximum altitude indicated in the table. However, in some cases there probably were sequential thermals during the time of ascent. Several clouds ascended to an inversion and remained roughly at the same altitude while new thermals ascended into the cloud. Indeed, the 0-dB*Z* echo developed in the clouds on 18 July after the clouds had reached the inversion. Similarly, the maximum reflectivity in the 5 August cloud observed at 1217–1245 increased from 0 to 15 dB*Z* while the cloud top remained between 2.7 and 3.0 km for 5 min. Cloud tops later ascended to 4 km and the reflectivity increased to 45 dB*Z* in a period of 10 min.

The ascent rate of the cloud tops determined from the sequential radar scans varied from about 2 to 8 $m\ s^{-1}$; the maximum updraft speed measured in the clouds by the C-130 was approximately twice the ascent rate of the tops.

The altitude of the top of the first 0-dB*Z* echo varied from about 2.0 to 4.1 km; 0 dB*Z* (on X band to avoid Bragg scatter) was chosen so as not to bias the results against weaker clouds while still being significantly beyond the reflectivity where calculations indicate that drops formed by coalescence dominate the radar echo. As can be seen from Table 1 and Fig. 2, there is a large variation in the maximum altitude of the 0-dB*Z* echo for a given maximum concentration of cloud droplets. There clearly is not a simple increase in the altitude with increase in N_{max}. For example in Table 1, $N_{max} \approx 1000\ cm^{-3}$ in the 20 July cloud and yet the altitude of the 0-dB*Z* echo is similar to that in the 4 August clouds where $N_{max} \approx 300\ cm^{-3}$. This result is not necessarily

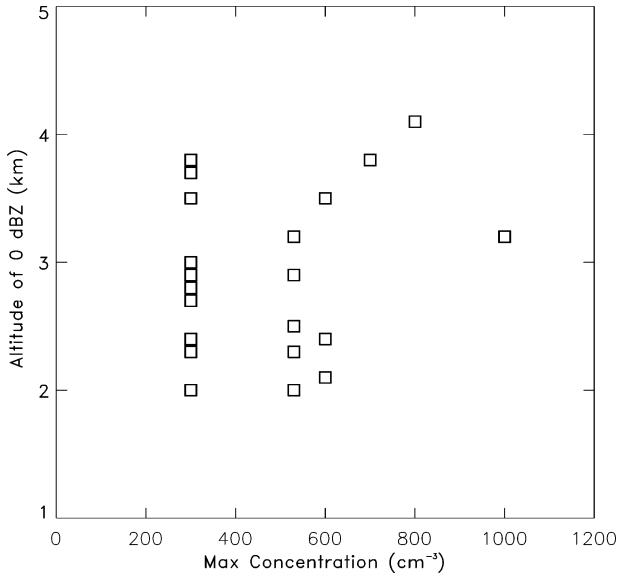

FIG. 2. Maximum concentration of cloud droplets measured on a particular day (N_{max}) vs the highest altitude of the first appearance of the 0-dBZ echo in different clouds. Data are taken from Table 1. The top of the echo is chosen since the hydrometeors constituting that part of the echo most likely came from below.

a contradiction of the classic prediction of Squires (1958) that clouds with higher drop concentrations (continental) are colloidally stable and are less likely to produce precipitation than their lower drop concentration (''maritime'') counterparts. The first appearance of the 0-dBZ echo in this study is most likely due to the formation of the first large drops that have undergone coalescence. However, as discussed by Lasher-Trapp et al. (2001), it is unknown whether or not the process responsible for the first drops that cause the early radar echo formation is important for the production of the main precipitation.

There was a tendency for the 0-dBZ echo to form at a higher altitude in clouds with higher ascent rates consistent with time being important in the coalescence process. However, the liquid water content along the trajectories of drops is probably the most important factor (Cooper et al. 1997). Figure 3 shows the ratio of liquid water content L to the adiabatic value L_{ad}, L/L_{ad}, versus altitude for the clouds observed on 20 and 24 July and 4 and 10 August, which are the clouds discussed below in section 5. The maximum values of L/L_{ad} are greater than 0.8 at almost all penetration levels on 4 and 10 August while $L/L_{ad} > 0.5$ in many regions of the 20 and 24 July clouds. Notice from Table 1 that the maximum reflectivity measured in the clouds in the latter two cases was only 0 dBZ, while it was 55 dBZ in the former cases. The maximum reflectivity was only 15 dBZ or less in all clouds with more than 600 cm^{-3}. Other clouds observed during the period between 19–24 July (not listed) did produce reflectivities of 40 dBZ or greater while cloud top was lower than the freezing level. The reflectivity was 30 dBZ or more in about half of the clouds with fewer than 600 cm^{-3}. There is clearly a range of maxima for the more maritime clouds illustrating that development of the radar reflectivity is likely more influenced by the dynamics than the cloud drop

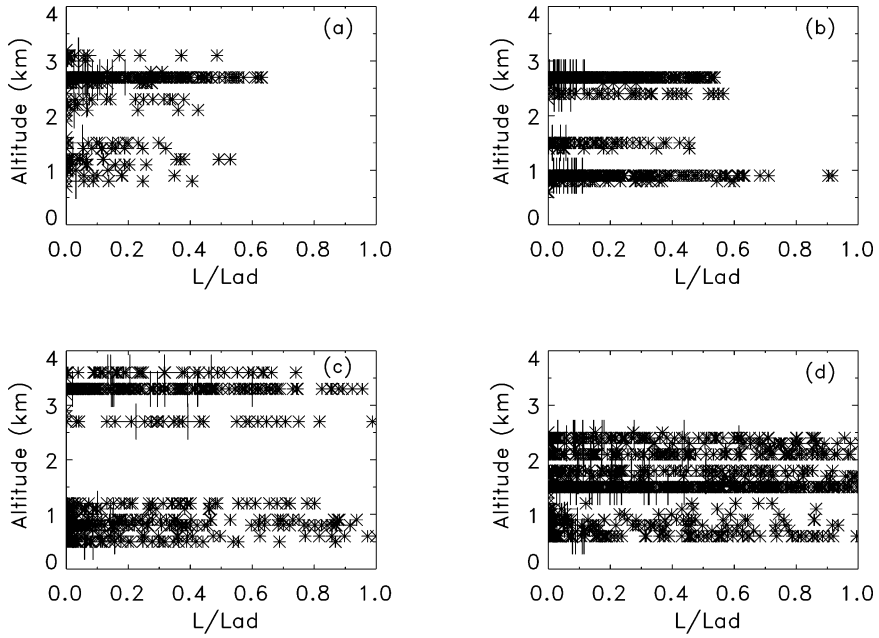

FIG. 3. Plots of 1-s average values of the ratio of liquid water content to the adiabatic value for all clouds sampled by the C-130 aircraft on (a) 20 and (b) 24 Jul, and (c) 4 and (d) 10 Aug 1995. The vertical lines are penetration averages.

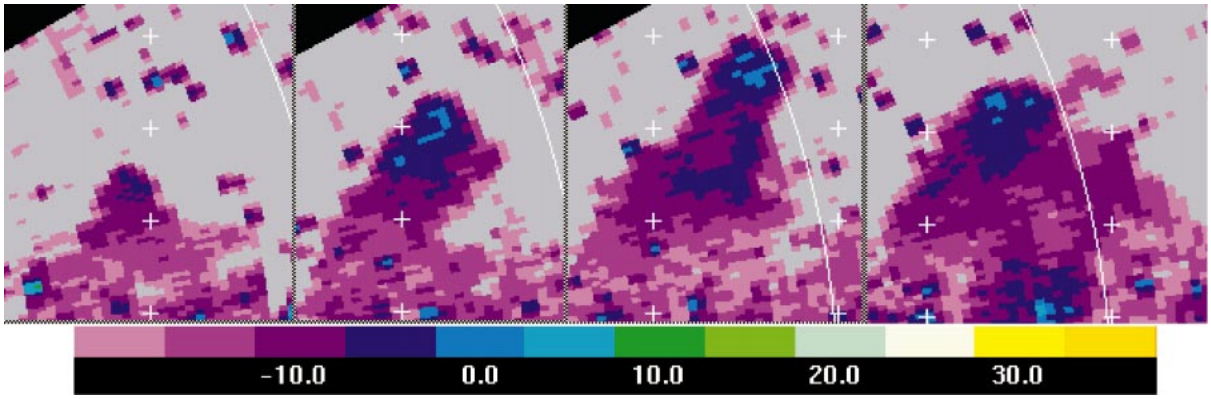

FIG. 4. X-band reflectivity at (far left) 1546:43 UTC; and 1550:27, 1552:52, and (far right) 1555:55 UTC on 20 Jul 1995. The horizontal and vertical tick marks are spaced at 2 and 1 km, respectively, with the lowest tick marks being at 1 km. The cloud was about 8 km south-southeast of the radar. The reflectivity scale is indicated along the bottom of the diagram.

number concentration. Probably the clearest relationship in the results shown in the table is that all the clouds with a maximum reflectivity of 55 dB*Z* have tops slightly greater than 5.5 km, just above the freezing level.

There is a significant spread in the 1-s values as well as the penetration averages of L/L_{ad} in Fig. 3. The averages at each level agree with the results presented by others (e.g., Blyth and Latham 1990) showing that generally the average value of L/L_{ad} does not decrease with height. The measurements on 4 and 10 August support the idea discussed by Blyth et al. (1988) that a core region of high liquid water exists inside a thermal for a significant fraction of its life. The picture is consistent with the radar observations presented in this study that showed the maximum reflectivity to be near cloud top and approximately equidistant from the horizontal edges in most cases. Adiabatic regions have been observed well above cloud base in this and other studies (e.g., Heymsfield et al. 1978; Jensen et al. 1985).

As can be seen from the table, there is a large variation in the average rate of increase of reflectivity for a given maximum concentration of cloud droplets. Indeed there is a large range of rates on a single day. The maximum rate was 5 dB*Z* min^{-1}, which corresponds to an increase in reflectivity from -10 dB*Z* to 40 dB*Z* in 10 min. The three highest values occurred on 10 August. A number of fractions contribute to this rate. The most important is the vigor of the cloud allowing persistence of high liquid water content.

5. Case studies

We now look at clouds that formed on 20 and 24 July and 4 and 10 August (Table 1) in more detail. The clouds were isolated and their tops ascended continuously for at least 1 km to the highest level. They also had continuous radar coverage during that period. The maximum concentration of cloud droplets ranged from 300 cm^{-3} on 4 August to 1000 cm^{-3} on 20 July. The ascent rate of the clouds was about the same on 20 July and 4 and 10 August, but was approximately double on 24 July.

a. Two cases with high concentrations of cloud droplets: The 20 and 24 July clouds

1) OBSERVATIONS

A sequence of RHIs is shown in Fig. 4 for the cloud observed on 20 July. As for the other cases, only the RHI with the maximum reflectivity is shown in the figure. The clouds were approximately the same width in the direction perpendicular to the one shown in the figure. The cloud top ascended from 2.5 to a maximum height of 4 km during the 6 min covered by the first three scans. It was collapsing by the time of the fourth scan. The maximum reflectivity only reached 0 dB*Z* and it did so first at an altitude of about 3 km near the top of the cloud (second scan in Fig. 4). The radar echo did not increase in intensity in the next two scans, presumably because the cloud liquid water content had been reduced as a result of entrainment and mixing. The rate of development of the radar echo between the first two scans was about 2.7 dB*Z* min^{-1}.

The maximum echo strength reached 5 dB*Z* in the 24 July cloud (Fig. 5) during the period the cloud top ascended to 4.2 km. There are no scans beyond the third one at 1633:41 UTC due to a radar malfunction. Again, only the RHI with the maximum reflectivity is shown and the cloud is the same size in both horizontal dimensions. The echo increased from -5 to 5 dB*Z* as the cloud top ascended from about 2.5 km to 4.2 km in 4.5 min at an average speed of about 5.5 m s^{-1}. The 0-dB*Z* echo formed in the upper regions of the cloud, between about 3 and 4 km, as the cloud top ascended. There is a single pixel of 5 dB*Z* in the center of the upper cap at 4 km in the last scan. As mentioned above, it is common for the maximum echo to be in this location suggesting that maximum growth occurs in a region of maximum liquid water content. The average rate of in-

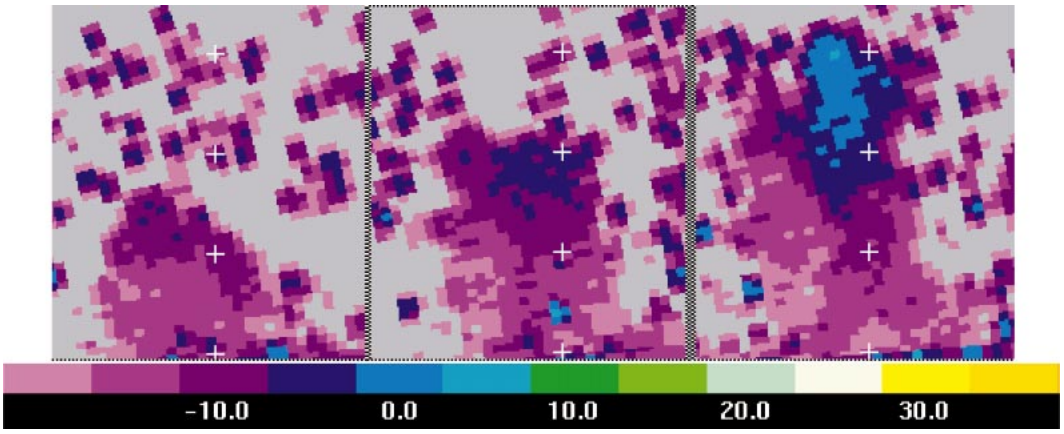

FIG. 5. X-band reflectivity at (left) 1629:12, (middle) 1631:26, and (right) 1633:41 UTC on 24 Jul 1995. The horizontal and vertical tick marks are spaced at 2 and 1 km, respectively, with the lowest visible tick marks at 1 km. The cloud was about 12 km southeast of the radar. The reflectivity scale is indicated along the bottom of the diagram.

crease of reflectivity was more than double the value for the 20 July cloud as seen in Table 1.

The C-130 made several penetrations of the 24 July cloud at about 2.4 km. Figure 6 shows the drop size distribution measurements from the FSSP and 260X probes on the C-130 at 1630:28 UTC in the region of cloud where the updraft speed $w > 3$ m s^{-1}. No drops were sampled by the 2DC probe. The penetration was about halfway between the first two scans shown in Fig. 5, probably missing the -5-dBZ echo. The peak updraft speed and liquid water content were about 8 m s^{-1} and 2.5 g m^{-3}, respectively. The reflectivity calculated from the size distribution is about -18 dBZ, significantly lower than the -10-dBZ value measured by the radar. The calculated reflectivity was dominated by the more numerous cloud drops detected by the FSSP. The step change of 100 μm suggests that larger drops may have been present, but were not measured by the instruments because of the small sample volumes. Unfortunately, the strongest echo region of this cloud (or any other discussed in this paper) was not penetrated by the C-130 aircraft, so the details of the particle size distribution responsible for the maximum radar reflectivity is unknown.

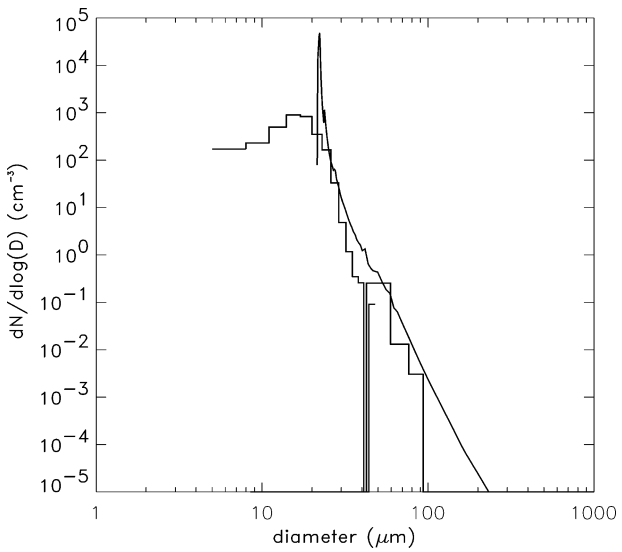

FIG. 6. Size distribution measured at 2.4 km on 24 Jul 1995 from 1630:28–1630:31 UTC with the FSSP and 260X probes on the C-130 (histogram), and the size distribution at 2.4 km calculated from the standard model run for 24 Jul (continuous line). The model liquid water content had an undilute value of 4 g m^{-3} and the average observed value was 1.8 g m^{-3}.

2) MODEL RESULTS

Figure 6 shows the drop size distribution calculated by the standard model run for 2.4 km on 24 July. There is reasonable agreement between the calculations and the observations (also shown in Fig. 6) particularly for the size range of 40 to 100 μm.

The altitude of the top and bottom of the observed maximum reflectivity are shown as a function of time for the 20 and 24 July clouds in Figs. 7a and 7b, respectively. The trajectory of the modeled cloud parcel along with the reflectivity values calculated from the standard, 3 m s^{-1} (on 20 July), and reduced-ugn model-run size distributions are also shown. As mentioned above, an updraft speed of 2 m s^{-1} from cloud base to the lowest level where observations were made was used unless otherwise specified. The model time elapsed from cloud base (about 550 m) to the first points shown in Figs. 7a and 7b are 970 and 590 s for the 20 and 24 July clouds, respectively.

The observed reflectivities on 20 July are significantly less at a particular altitude in all scans than the standard run model values. They are greater in the first scan however than the reduced-ugn model-run values. There is reasonable agreement between the reflectivity values from the 3 m s^{-1} model run and the observed maximum

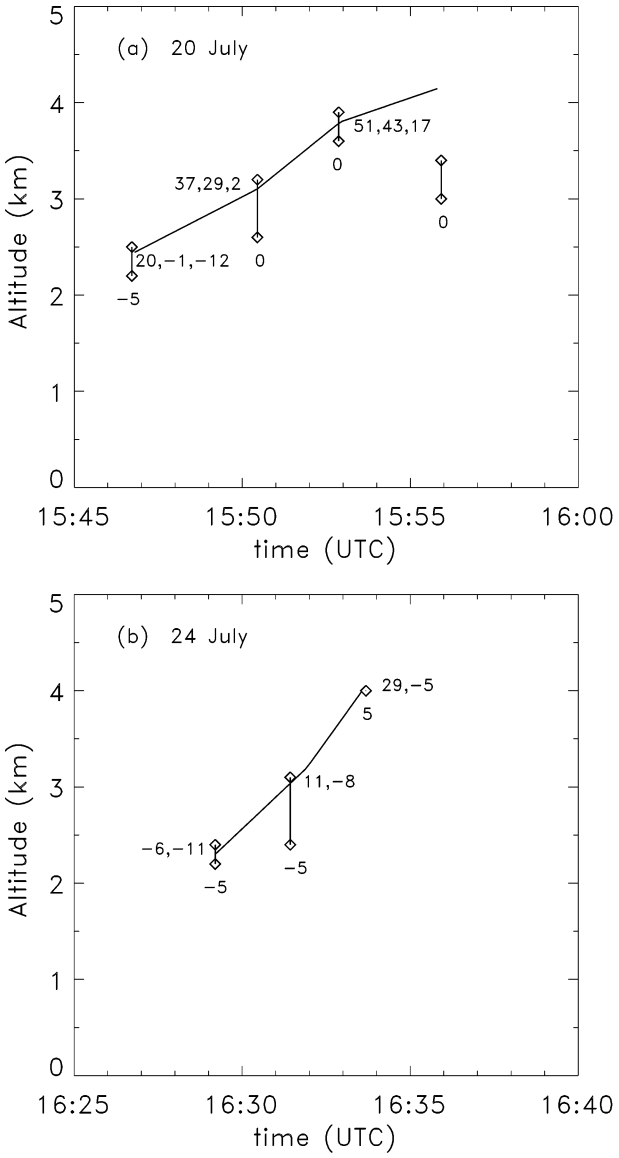

FIG. 7. The ◇ symbols represent (a) the top and (b) the bottom altitudes of the observed maximum reflectivity as a function of time and height for the 20 and 24 Jul clouds, respectively, obtained from Figs. 4 and 5. The single numbers below the points are the value of the maximum reflectivity at the given time. The solid curve is the height of the modeled parcel. The three numbers in (a) are the model reflectivities for the standard, 3 m s^{-1}, and reduced-ugn runs; only the standard and reduced-ugn model reflectivities are shown in (b).

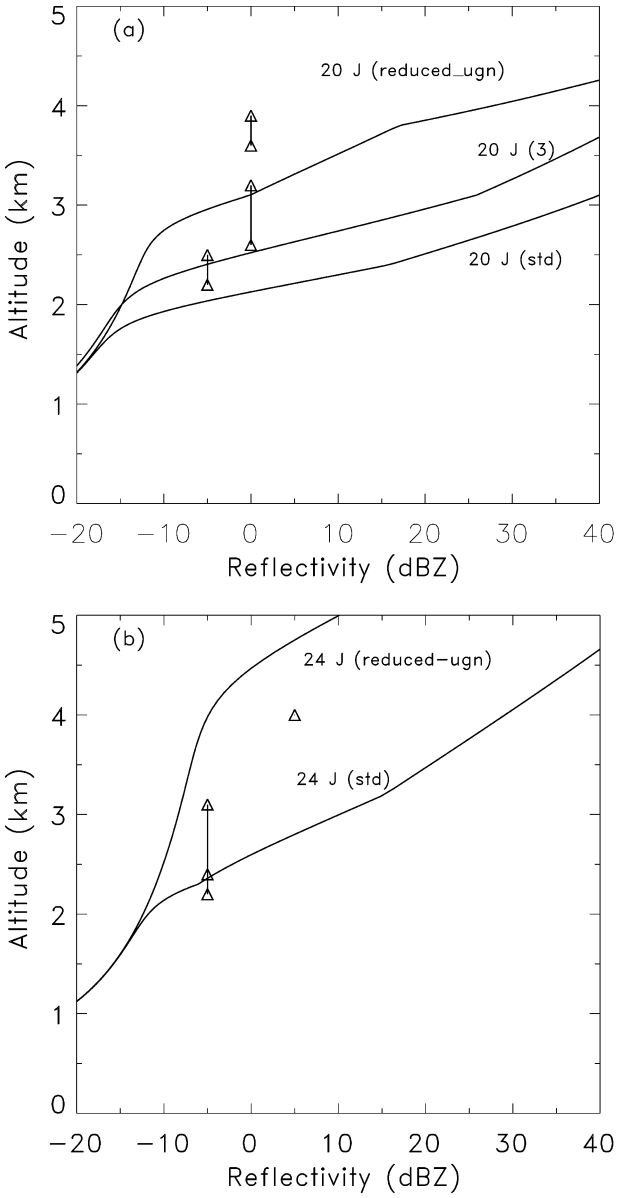

FIG. 8. (a), (b) Altitudinal range of the observed maximum reflectivity (Δ symbols) and the model reflectivities (solid curves) plotted vs altitude for the 20 and 24 Jul clouds, respectively. Note that the top of the −5-dBZ echo in the first scan on 24 Jul [in (b)] is at the same altitude as the bottom of the −5-dBZ echo in the second scan. The curves in (a) are for three model runs on 20 Jul: 20 J (std) and 20 J (reduced-ugn) are for the standard and reduced-ugn runs, respectively; and 20 J (3) is for the standard run, but with an updraft speed of 3, rather than 2 m s^{-1} in the lowest kilometer of cloud. The curves in (b) are for the standard (24 J std) and reduced-ugn (24 J reduced-ugn) runs for the 24 Jul cloud.

values in the first scan. The magnitude of the differences can be clearly seen in Fig. 8a, which shows the observed maximum and calculated reflectivities plotted versus altitude. The observed maximum reflectivities and their vertical extent are indicated by the triangles joined by a vertical line and the model values for the three runs are shown by the solid-line curves. There is a marked change in slope of the model curves at about −10 dBZ as the dominant growth mode changes from condensation to coalescence. The calculated −5-dBZ reflectivity was attained between 200 and 500 m below the observed altitudes in the standard run. The figure also illustrates that an increase of 1 m s^{-1} in the low-level ascent rate produces an increase of about 400 m in the altitude of the 0-dBZ echo, or put another way, a reduction in reflectivity of about 20 dBZ at the constant

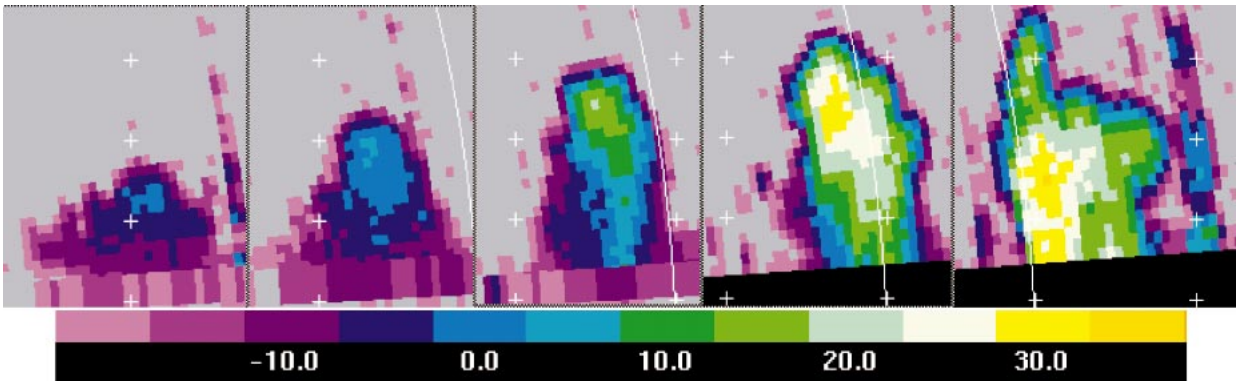

FIG. 9. Five vertical scans through a cloud on 10 Aug at (beginning on the left) 1456:00, 1458:15, 1500:30, 1502:27, and 1506:39 UTC. The vertical and horizontal scales are 1 and 2 km, respectively with the lowest tick marks at 1 km. The radar top is just less than 3 km in the first scan. The cloud was approximately 19 km to the south-southeast of the radar. The first scan of this cloud at 1453:39 UTC is not shown here. The reflectivity scale (shown below the scans) increments by 5 dB*Z*.

altitude of 2.5 km. This sensitivity to the low-level ascent rate is greatly reduced in the reduced-ugn run presumably because growth is dominated by condensation, which does not depend on the updraft speed.

The model reflectivity compares well with the observed value in the first scan of the 24 July cloud. The curve representing the results of the standard model run, shown in Fig. 8b, passes through the top of the first observed −5-dB*Z* echo. The observed reflectivity did not increase as the cloud top ascended to just above 3 km; such behavior cannot be reproduced in the simple parcel model.

The diagrams in Figs. 7 and 8 indicate that the first −5-dB*Z* echo in the 20 and 24 July clouds is entirely explainable with ordinary collision and coalescence, which includes giant and ultragiant nuclei within sensible limits of the low-level updraft speed. The reduced-ugn model runs do not explain the observations.

The observed reflectivities are significantly less than the standard model run reflectivities for values of 0 dB*Z* and greater in both cases. This is most likely because of the reduction in liquid water content. For example, the cloud on 20 July was obviously substantially subadiabatic between the second and third scans since the maximum reflectivity did not increase (Fig. 4 and Figs. 7 and 8). The cloud decayed after the last scan shown.

The cloud droplet number concentrations observed on 20 and 24 July were approximately the same (1000 and 800 cm^{-3}, respectively) and yet the model reflectivity values in the 24 July standard run were generally less than those for the 20 July run at a given altitude, presumably because there is less time available for coalescence growth in the stronger updrafts of the 24 July case. The result does not agree with the observations of the two clouds, however (Figs. 4, 5, 7, and 8), probably because cloud liquid water content plays such an important role in coalescence growth. The change in slope of the reflectivity–altitude curves in Fig. 8 occur at a higher altitude in the reduced-ugn runs because coalescence does not dominate until later.

b. Two cases with medium concentrations of cloud droplets: The 4 and 10 August clouds

1) OBSERVATIONS

Figure 9 shows a sequence of RHIs with the maximum reflectivity from the cloud on 10 August that was discussed by Cooper et al. (1996). The cloud top ascended 1.8 km in about 6 min to a height of 4.5 km. The 30-dB*Z* echo developed at about 3.3 km just as the cloud reached its maximum height. The reflectivity increased to 35 dB*Z* as the 30 dB*Z* echo descended. The cloud started to decay soon thereafter. The maximum reflectivity was −5 dB*Z* and cloud top was 2.2 km in the scan before the first one shown (1453:39 UTC) in Fig. 9, so the reflectivity increased from −5 to 30 dB*Z* in just under 9 min. As in the previous two examples, the maximum radar echo developed in the center of the upper region of the cloud.

Notice in Fig. 9 that a ''shaft'' of up to 5 dB*Z* had descended to the lowest levels at 1500:30 UTC (third frame). Thus the ''first precipitation'' fell out of the cloud about 6 min after the cloud top passed 2 km, and about 10 min after the first appearance of −10 dB*Z*. The 30-dB*Z* echo reached the lowest level approximately 5 min later. This illustrates the problem with statements about the ''time to rain.'' The maximum echo at the lower levels is no longer in the center of the cloud.

The C-130 penetrated approximately the same region of the cloud at an altitude of 1.7 km at 1501, corresponding most closely to the third panel in Fig. 9. The maximum radar reflectivity at that altitude is seen to be 5 dB*Z* associated with the ''rain shaft'' mentioned above. The measurements, illustrated in Fig. 10, indicate a 1-km region with liquid water content near the value expected for adiabatic ascent. The updraft is highly variable across this region, however. Within the cloud, the radar reflectivity calculated from the 260X data tends to be significantly lower in the regions of strongest updraft than in regions of downdraft or weaker updraft. Drop diameters up to about 500 μm are found in these

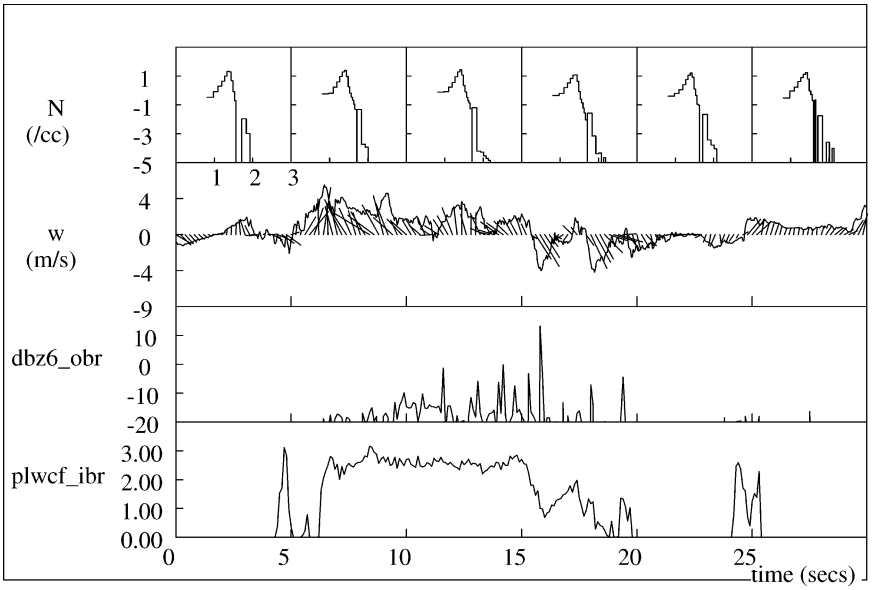

FIG. 10. The C-130 aircraft gathered 10-Hz data 1501:30 UTC 10 Aug 1995. (top to bottom) 10-s average size distribution from the FSSP and 260X for the period below the box; vertical wind speed (w) superimposed with wind vectors calculated from the vertical wind and horizontal wind along the direction of motion; reflectivity (dbz6_obr; in dBZ) calculated from the 260X size distribution; and liquid water content (plwcf_ibr; in g m^{-3}) calculated from the FSSP size distribution.

latter regions with calculated reflectivities of about 10 dBZ. This agrees reasonably well with the reflectivity in the rain shaft measured by the radar at 1.7 km at 1500:30 UTC. Figure 11 shows details of a penetration made 4 min later again through the same region of the cloud as shown in Fig. 9 at approximately the same altitude. It appears that the aircraft penetrated a fresh turret that was ascending through older cloud. The liquid water content is substantially less everywhere except in the narrow updraft where it is more than 3.5 g m^{-3}. The maximum updraft speed is 8 m s^{-1} and the reflectivity is about -10 dBZ due to the cloud droplets. The updraft is bounded on either side by substantial downdrafts; the transitions between the updraft and downdraft are marked by significant changes in liquid water content and the reflectivity calculated from the 260X probe. The

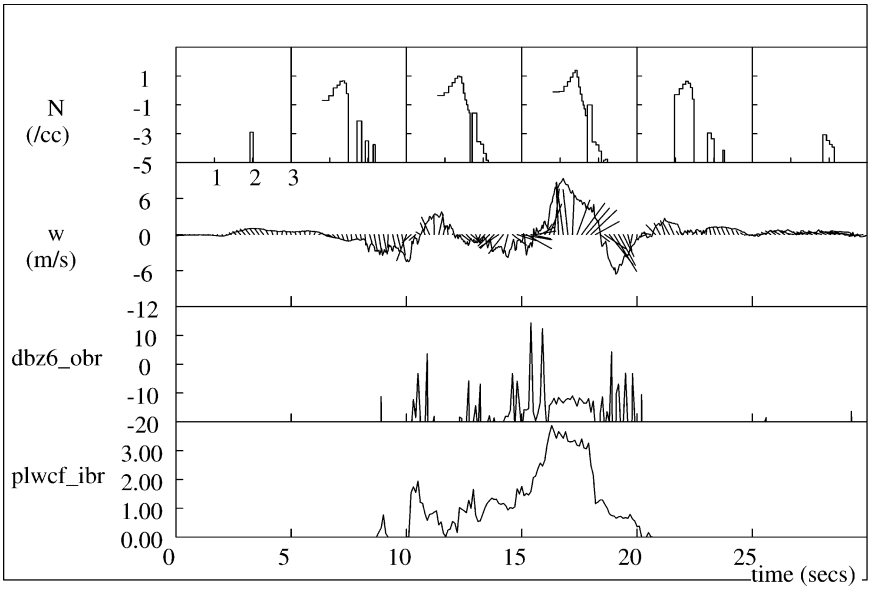

FIG. 11. As in Fig. 10, but for a start time of 1504:50 UTC on 10 Aug.

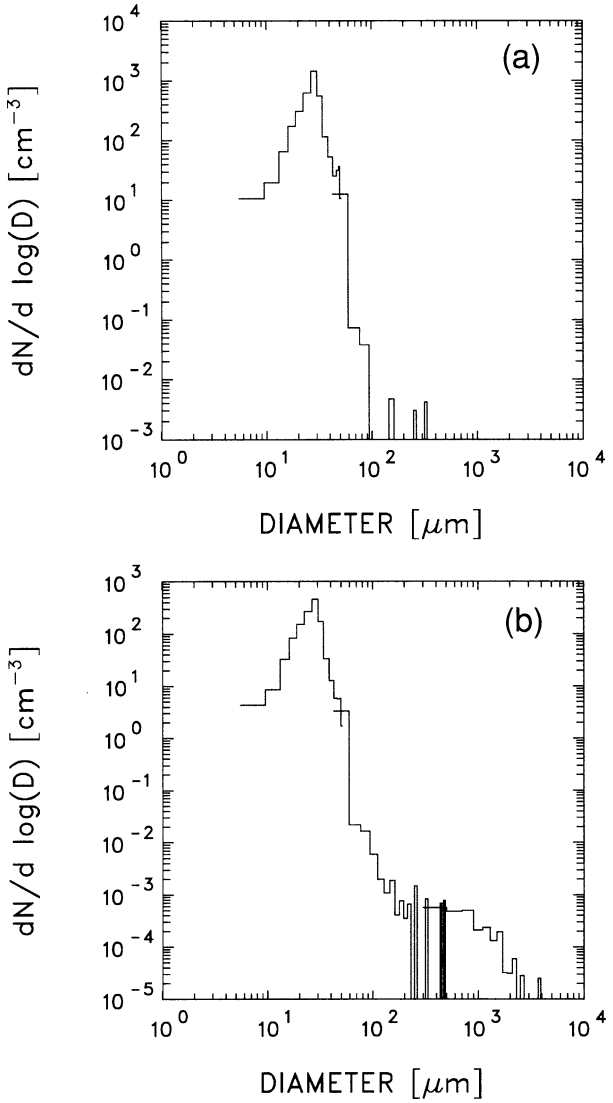

FIG. 12. Size distributions measured at an altitude of 1.8 km on 10 Aug 1995 at (a) 1505:07–1505:09 (updraft) and (b) 1505:00–1505:20 UTC (entire cloud) with the FSSP, 260X, and 2DP probes. Note that no particles were detected by the 2DP during the first time period. The average values of the liquid water content measured in (a) and (b) were 3.0 g m^{-3} and 1.5 g m^{-3}, respectively.

reflectivity again is up to about 10 dB*Z* in the downdrafts. The size distributions averaged over the updraft and the entire penetration (shown in Figs. 12a and 12b, respectively) clearly show that, at this low altitude, there are larger particles of up to 1-mm diameter in the downdrafts and in weaker regions of updraft. These observations and the radar scans at 1502:27 and 1506:39 UTC all suggest that millimeter-sized drops were present at the altitude of the strongest echo (about 3.5 km) and were sedimented and/or transported in the downdrafts to the aircraft penetration level.

The radar reflectivities measured in the five clouds tracked by the radar on 4 August listed in Table 1, were generally less than those measured at the same altitude in the clouds on 10 August. Figure 13 shows a sequence of RHIs with maximum reflectivity from 1458 to 1508 UTC for one cloud on 4 August. It attained a maximum reflectivity of 15 dB*Z* and the 0-dB*Z* echo first formed between 3 and 4 km. Radar tops were similar in the 4 and 10 August cases, as were the cloud-top ascent rates measured by radar and the maximum concentration of cloud drops measured by the aircraft (see Table 1). The other clouds on 4 August behaved in a similar fashion, although there was considerable variability.

Figure 14 illustrates a size distribution measured near the top of a cloud on 4 August that had reached its maximum height. The distribution is similar to one obtained by averaging over all penetrations made at about 3.5 km with $w > 5$ m s^{-1}. The reflectivity calculated from the observed distribution is comparable to that measured by the radar. Notice that the concentration of drizzle drops (diameter, between about 50 and 100 μm) is significantly greater than in the spectrum measured in the 10 August cloud (Fig. 12b), which gives a similar reflectivity.

2) MODEL RESULTS

Time–height diagrams showing the altitude range of the maximum reflectivity are shown in Figs. 15a and 15b for the 10 and 4 August, respectively. The trajectory of the modeled cloud parcel annotated with the reflectivity values from the standard and reduced-ugn model runs are also shown. The reflectivities from the reduced-ugn model run are significantly less than all the observed values for the 10 August case. This is also illustrated in the diagrams shown in Fig. 16a of the observed maximum reflectivity versus altitude and the reflectivity from the standard and reduced-ugn model runs. The observed -5-dB*Z* echoes on 4 August (Fig. 16b) lie between the results from the standard and reduced-ugn run. Note that, while the reduced-ugn model-run reflectivity value at 2.2 km (-8 dB*Z*) is significantly closer to the observed value of -5 dB*Z* than the standard run value (7 dB*Z*), the -5-dB*Z* reflectivity value occurs at a much higher altitude for the reduced-ugn run than the observed value compared to the standard run.

The 0- and 5-dB*Z* reflectivities in the 4 August cloud are at a higher altitude probably because of reduced liquid water content. Figure 13 shows that the cloud was considerably narrower than the one on 10 August, so the erosion of the core probably occurred at a lower altitude. The -5-dB*Z* echo on 10 August was first observed at about 2 km whereas the altitude calculated in the standard model run was 2.2 km. The standard run reflectivity value at 2 km, however, is -11 dB*Z*. The cloud was known to exist at low levels for about 15 min, so a run was made with an updraft of 1.5 m s^{-1} below 1.7 km; the curve representing the results passes through the -5-dB*Z* point.

The increase in altitude between the 0- and 5-dB*Z*

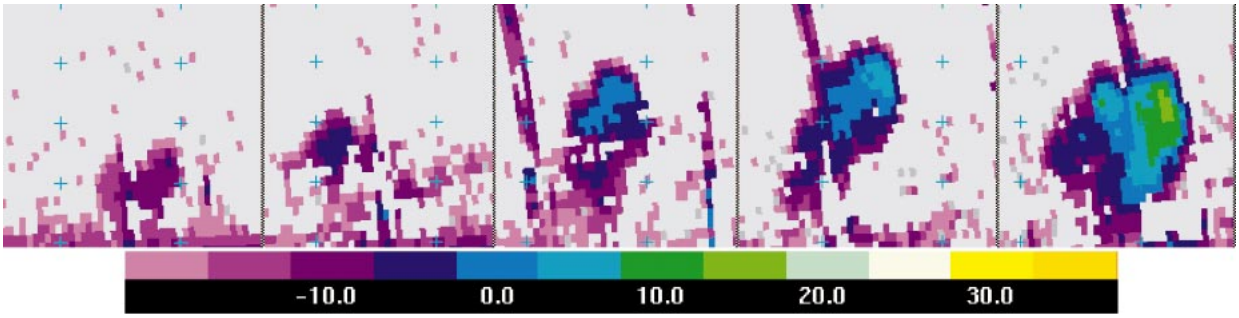

FIG. 13. Five vertical scans through a cloud on 4 Aug at (far left) 1458:08 UTC; and 1500:24, 1502:53, 1505:22, and (far right) 1507:45 UTC. The vertical and horizontal scales are 1 and 2 km respectively with the lowest tick marks at 1 km. The cloud was approximately 22 km to the south of the radar. The reflectivity scale (shown below the scans) increments by 5 dB*Z*.

echoes on 10 August is larger than for the calculations, again probably due to entrainment. The altitude change between the 5- and 20-dB*Z* echo, however, is approximately the same as the calculated value. This would occur if a new thermal containing close to adiabatic liquid water content passed through the cloud. Figure 11 shows an example of such a thermal at 1.8 km.

The results indicate that the first −5-dB*Z* echo in the 4 and 10 August clouds can also be explained with ordinary collision and coalescence that includes giant and ultragiant nuclei. The altitude of the first −5-dB*Z* echo observed in the 4 August cloud lies between the values calculated from the standard and reduced-ugn model runs, so again, the reduced-ugn model runs do not explain the observations. It is clear from the model results from these cases and the 20 and 24 July cases, that reasonable variation in any one of the three variables on which the increase of reflectivity with height depends—liquid water content, low-level updraft speed, or the giant and ultragiant nucleus size distribution—could be made to decrease the disparity between the model results and observations.

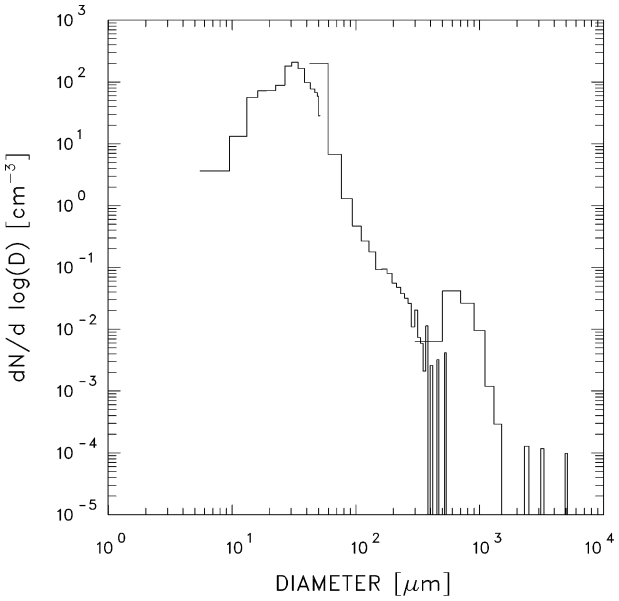

FIG. 14. Size distribution measured at an altitude of 3.6 km on 4 Aug 1995 at 1513:25–1513:30 UTC with the FSSP, 260X, and 2DP probes on board the C-130. The average value of liquid water content was 1.0 g m^{-3}.

The size distribution from the standard model run at 1.8 km, 10 August (Fig. 17a) contains fewer drizzle drops than the observed distribution. The observed size distribution of cloud droplets is also much broader than the model distribution. The size distribution corresponding to the observed maximum reflectivity aloft of 30 dB*Z* calculated from the standard model run is shown in Fig. 17b. It can be seen that the large end of the model size distribution at 3.3 km is similar to the observed size distribution at 1.8 km, thus lending support to the argument that drops with diameters of at least 1 mm could be produced in the upper levels of the cloud to subsequently sediment to the lower levels of the cloud.

Figures 18a and 18b show the size distributions produced by the standard and reduced-ugn model runs for 4 August at 3.6 km. The former compares well with the observed distribution shown in Fig. 14, particularly for drizzle-size drops. The correct size of the observed largest drops are also reproduced, although there are clearly significant sampling errors due to the instrument sample volume. Sedimentation also contributes to the problem of comparing observations and model results. The reduced-ugn model run produced fewer large drops than were observed.

6. Conclusions and discussion

We have examined the early development of warm, Florida cumulus clouds that were observed with radar and aircraft during SCMS. The principal conclusion of this study is that coalescence growth on giant and ultragiant nuclei is sufficient to explain the observations. The observations do not suggest that effects like enhanced collision efficiencies due to turbulence are required. This conclusion is consistent with the UGN hypothesis proposed by Johnson (1982). Indeed, the mea-

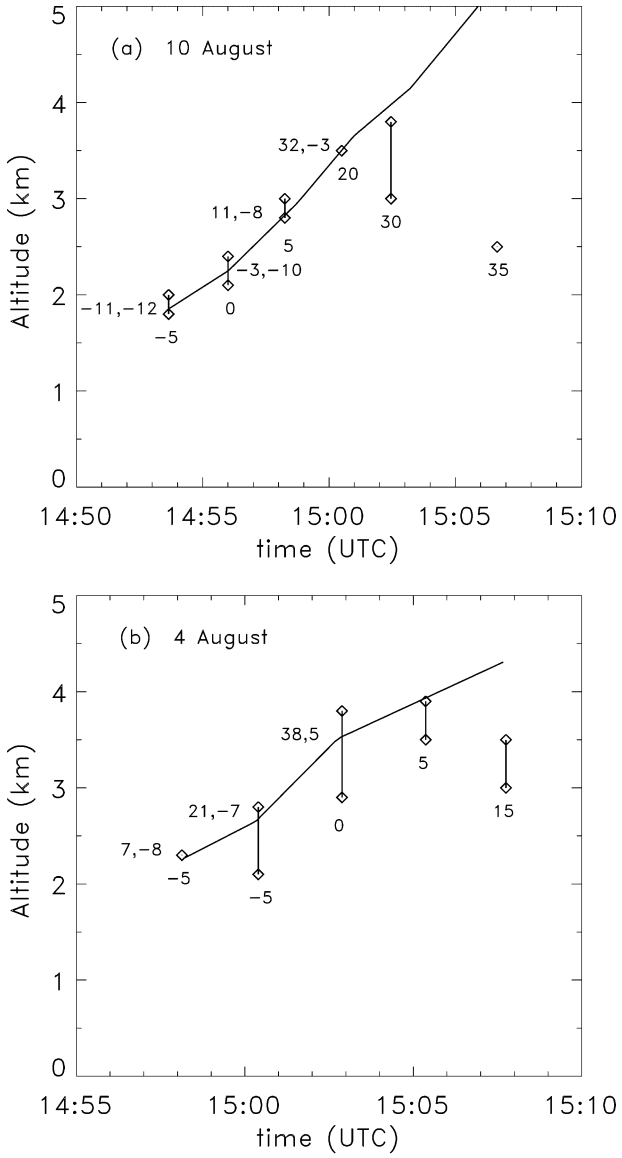

FIG. 15. Similar to Fig. 7, but for clouds on (a) 10 Aug and (b) 4 Aug. The two numbers alongside the curves are the reflectivity values for the standard and reduced-ugn model runs.

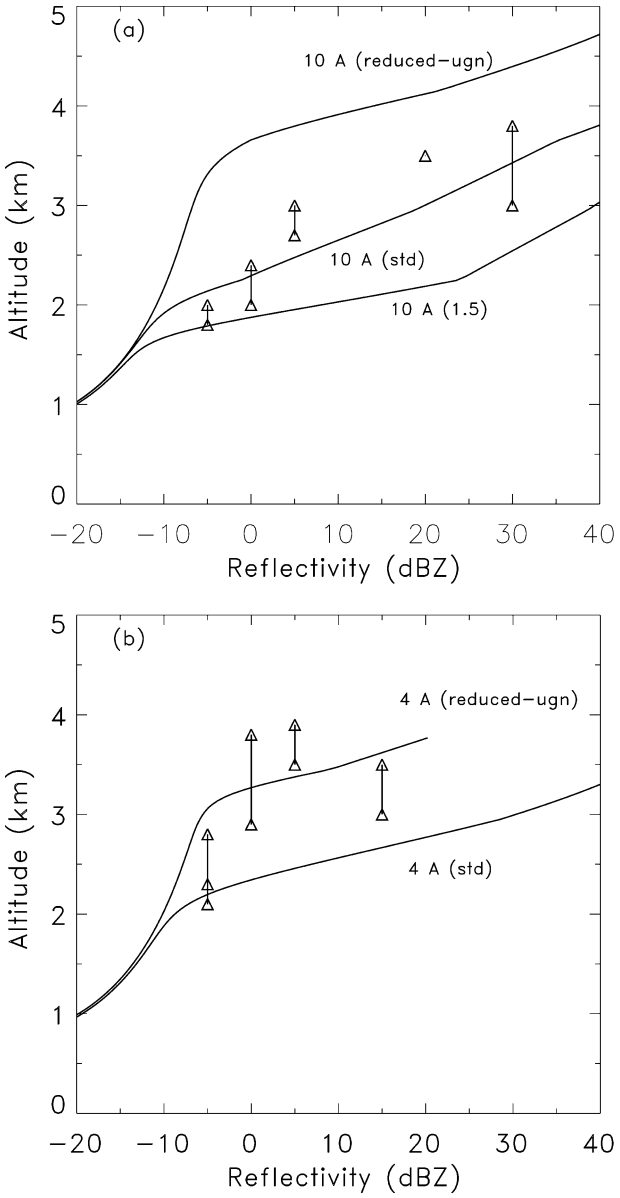

FIG. 16. Similar to Fig. 8, but for clouds on (a) 10 Aug and (b) 4 Aug. The curve marked "1.5" in (a) is for the standard run, but with a low-level (altitude $z < 1.7$ km) updraft of 1.5 m s^{-1}. Only standard and reduced-ugn runs were made for the 4 Aug case.

surements of Woodcock (1953) suggest that there may be an even greater concentration of giant and ultragiant nuclei in the marine environment than used here. The results are consistent with the conclusions of Cooper et al. (1996) and they support the conclusion from the combined radar and theoretical study of Caylor and Illingworth (1987).

It is impossible to know if the inclusion of turbulent capture, enhancement due to mixing, or van der Waals forces in the reduced-ugn runs might have produced the same result as including UGN without these effects. However, the data do not force one to look in these directions for explanations of early radar echo formation in cumulus. The most intense first echoes were almost entirely in the upper center of the ascending turrets, so the most straightforward hypothesis is to look for straightforward answers in the large end of the aerosol size spectrum. It is this that really needs a better quantitative test than was possible from SCMS data to see if any fundamentally different kinds of explanations will be needed or not. The results from this paper suggest that they may not.

There was no evidence from the observations of a simple relationship between the concentration of cloud droplets and the altitude of the first 0-dBZ echo. Indeed, it is clear from the calculations presented in Figs. 7, 8,

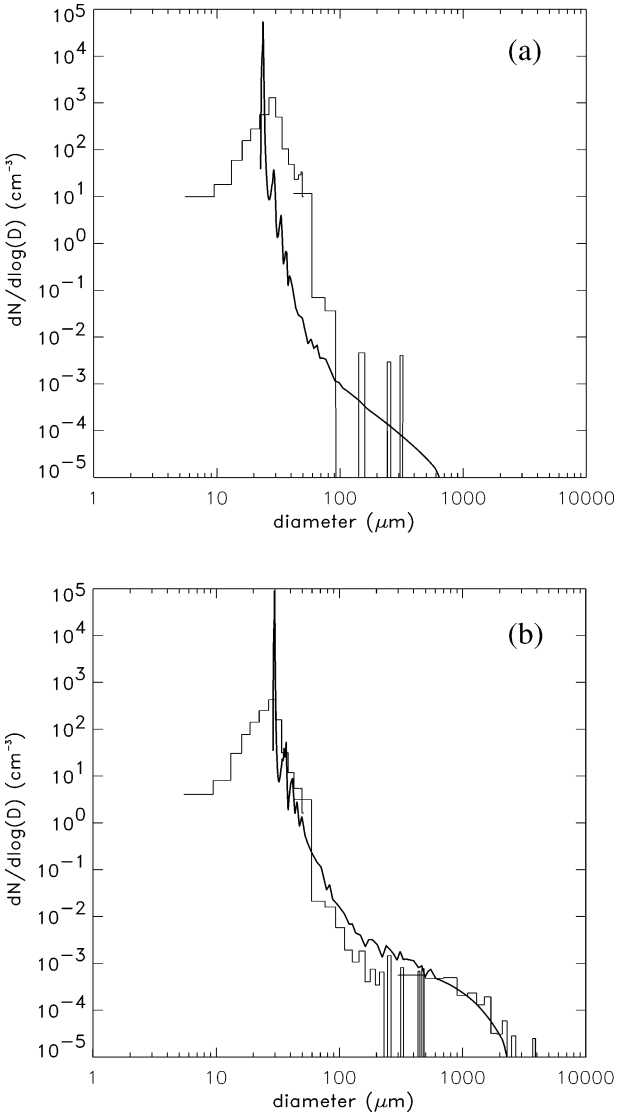

FIG. 17. Size distribution at (a) 1.8 km and (b) 3.3 km produced from the standard model run for 10 Aug 1995 with a low-level updraft of 1.5 m s^{-1} and with giant and ultragiant nuclei. The values of the liquid water content are 3.4 and 6 g m^{-3} (undiluted values) for (a) and (b), respectively. The observations shown in Fig. 12 are superimposed.

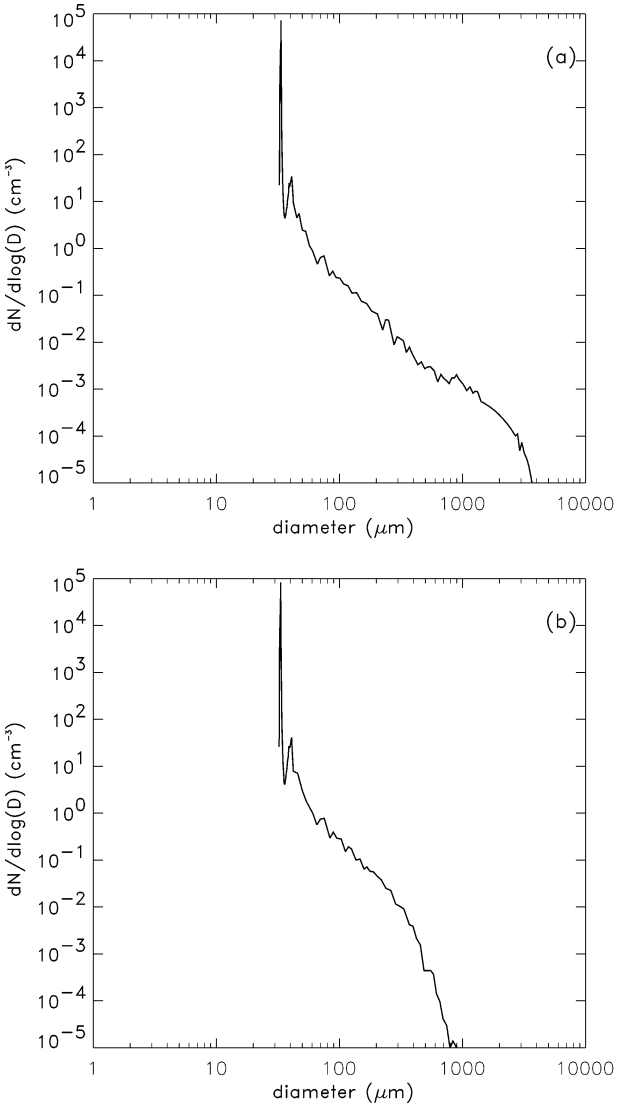

FIG. 18. Size distributions at 3.6 km produced from the model for (a) the standard run and (b) the reduced-ugn run for 4 Aug 1995. The liquid water content is the undiluted value of 6.2 g m^{-3}.

15, and 16 that a more significant influence on the value of reflectivity at a particular altitude in an adiabatic core is the amount of time available for growth. The altitude of the 0-dBZ reflectivity is calculated to occur at about the same altitude for the 20 July and 4 August cases, which had similar updraft speeds but with $N_{\max} = 1000$ and 300 cm^{-3} for 20 July and 4 August, respectively. This is a consequence of the fact that reflectivity is a function of D^6 and the same ultragiant nuclei distribution is used in all cases. This does not imply that the classic prediction first pointed out by Squires (1958) and discussed recently by Rosenfeld (1999) and Hudson and Yum (2001) that clouds with a higher concentration of drops are more colloidally stable is incorrect, since the continued production of warm rain may be unrelated to the development of the first radar echoes that we have studied in this paper. Hudson and Yum found more drizzle in SCMS maritime clouds than in the continental clouds, which seemed to be a result of reduced number of cloud condensation nuclei rather than to increased number of giant nuclei. The results of this paper are not necessarily in conflict with Hudson and Yum's results, because their analysis pertained to drizzle concentrations measured from aircraft (defined there as drops with diameter >50 μm) while this paper is concerned with first echo formation, influenced by the presence of the largest and perhaps the fewest drops. As mentioned above, although the first radar echoes can be explained by using giant and ultragiant nuclei, it is not clear if

these particles are numerous enough to explain the subsequent progression to a rain shower. The results of the modeling study of Lasher-Trapp et al. (2001) suggest that the first echo formation and overall rainfall production may be unrelated if UGN are present. It is entirely possible that some other enhanced-growth mechanism is required. In fact, the results presented by Cooper et al. (1997) suggest that the presence of UGN may limit the formation of drizzle particles ($r \approx 100$ μm) by decreasing the overall droplet concentration, implying that UGN may well have a detrimental affect on warm rain formation. Further study is required.

There is a stronger relationship between the altitude of the first 0-dB*Z* echo and the concentration of cloud drops according to the model if the larger nuclei are excluded from the initial size distribution. This can be seen by comparing the reduced-ugn runs for 20 July and 4 August (Figs. 8a and 16b, respectively). Johnson (1982), who was one of the first to show this result, found that truncating the maritime size distribution had very little effect on the time taken for the reflectivity to increase to 20 dB*Z*, for example, whereas it had a dramatic effect on the continental size distribution.

A more difficult problem to address is how to measure the larger nuclei with an aircraft. It is clear from this study, which has made use of the best measurements available, that further progress in describing and parameterizing the warm rain process depends on being able to reliably measure the giant and ultragiant nuclei.

Acknowledgments. We wish to thank the many people involved in SCMS, particularly the personnel in ATD at NCAR. We are grateful for the use of the NCAR computers provided by the Scientific Computing Division. This work was supported by the National Science Foundation under Grants ATM-9420333, ATM-9707301, and ATM-9981937; and by the Hadley Centre, Met Office, United Kingdom. Part of this research was performed while the first author was on sabbatical leave in the Department of Pure and Applied Physics, UMIST, and the Department of Meteorology, University of Edinburgh.

REFERENCES

Baumgardner, D., and M. Spowart, 1990: Evaluation of the Forward Scattering Spectrometer Probe. Part III: Time response and laser inhomogeneity limitations. *J. Atmos. Oceanic Technol.,* **7,** 666–672.

——, and A. Korolev, 1997: Airspeed corrections for optical array probe sample volumes. *J. Atmos. Oceanic Technol.,* **14,** 1224–1229.

——, W. Strapp, and J. E. Dye, 1985: Evaluation of the Forward Scattering Spectrometer Probe. Part II: Corrections for coincidence and dead-time losses. *J. Atmos. Oceanic Technol.,* **2,** 626–632.

Beard, K. V., and H. T. Ochs III, 1993: Warm-rain initiation: An overview of microphysical mechanisms. *J. Appl. Meteor.,* **32,** 608–625.

Blyth, A. M., and J. Latham, 1990: Airborne studies of altitudinal variability in the microphysical structure of non-precipitating, ice-free, Montanan cumulus. *Quart. J. Roy. Meteor. Soc.,* **116,** 1405–1423.

——, W. A. Cooper, and J. B. Jensen, 1988: A study of the source of entrained air in Montana cumuli. *J. Atmos. Sci.,* **45,** 3944–3964.

Carpenter, R. L., K. K. Droegemeier, and A. M. Blyth, 1998: Entrainment and detrainment in numerically simulated cumulus congestus clouds. Part I: General results. *J. Atmos. Sci.,* **55,** 3417–3432.

Caylor, I. J., and A. J. Illingworth, 1987: Radar observations and modelling of warm rain initiation. *Quart. J. Roy. Meteor. Soc.,* **113,** 1171–1191.

Cooper, W. A., 1988: Effects of coincidence on measurements with a forward scattering spectrometer probe. *J. Atmos. Oceanic Technol.,* **5,** 823–832.

——, C. A. Knight, J. L. Brenguier, 1996: Observed vs calculated rates of growth by coalescence. *Proc. 12th Int. Conf. on Cloud and Precipitation,* Zurich, Switzerland, ICCP, 53–56.

——, R. T. Bruintjes, and G. K. Mather, 1997: Some calculations pertaining to hygroscopic seeding with flares. *J. Appl. Meteor.,* **36,** 1449–1469.

de Leeuw, G., 1986: Vertical profiles of giant particles close above the sea surface. *Tellus,* **38B,** 51–61.

Dye, J. E., and D. Baumgardner, 1984: Evaluation of the forward scattering spectrometer probe. Part I: Electronic and optical studies. *J. Atmos. Oceanic Technol.,* **1,** 329–344.

Exton, H. J., J. Latham, P. M. Park, S. J. Perry, M. H. Smith, and R. R. Allan, 1985: The production and dispersal of marine aerosol. *Quart. J. Roy. Meteor. Soc.,* **111,** 817–837.

Heymsfield, A. J., P. N. Johnson, and J. E. Dye, 1978: Observations of moist adiabatic ascent in northeast Colorado cumulus congestus clouds. *J. Atmos. Sci.,* **35,** 1689–1703.

Hu, Z., R. T. Bruintjes, and E. A. Betterton, 1998: Sensitivity of cloud droplet growth to collision and coalescence efficiencies in a parcel model. *J. Atmos. Sci.,* **55,** 2502–2515.

Hudson, J. G., and S. S. Yum, 2001: Maritime-continental drizzle contrasts in small cumuli. *J. Atmos. Sci.,* **58,** 915–926.

Jensen, J. B., P. H. Austin, M. B. Baker, and A. M. Blyth, 1985: Turbulent mixing, spectral evolution and dynamics in a warm cumulus cloud. *J. Atmos. Sci.,* **42,** 173–192.

Johnson, D. B., 1982: The role of giant and ultragiant aerosol particles in warm rain initiation. *J. Atmos. Sci.,* **39,** 448–460.

Knight, C. A., and L. J. Miller, 1993: First radar echoes from cumulus clouds. *Bull. Amer. Meteor. Soc.,* **74,** 179–188.

——, and ——, 1998: Early radar echoes from small, warm cumulus: Bragg and hydrometeor scattering. *J. Atmos. Sci.,* **55,** 2974–2992.

——, J. Vivekanandan, and S. G. Lasher-Trapp, 2002: First radar echoes and the early Z_{DR} history of Florida cumulus. *J. Atmos. Sci.,* **59,** 1454–1472.

Laird, N. F., H. T. Ochs III, R. M. Rauber, and L. J. Miller, 2000: Initial precipitation formation in warm Florida cumulus. *J. Atmos. Sci.,* **57,** 3740–3751.

Lasher-Trapp, S. G., C. A. Knight, and J. M. Straka, 2001: The formation of early radar echoes from ultragiant aerosol: Modeling and observations. *J. Atmos. Sci.,* **58,** 3545–3562.

——, W. A. Cooper, and A. M. Blyth, 2002: Measuring ultragiant aerosol in the atmosphere from aircraft-mounted optical array probes: Difficulties and probability-based estimates. *J. Atmos. Oceanic Technol.,* **19,** 402–408.

Mészáros, A., and K. Vissy, 1974: Concentration, size distribution and chemical nature of atmospheric aerosol particles in remote oceanic areas. *J. Aerosol Sci.,* **5,** 101–109.

Ochs, H. T., III, and R. G. Semonin, 1979: Sensitivity of a cloud microphysics model to an urban environment. *J. Appl. Meteor.,* **18,** 1118–1129.

O'Dowd, C. D., M. H. Smith, I. E. Consterdine, and J. A. Lowe, 1997: Marine aerosol, sea-salt, and the marine sulphur cycle: A short review. *Atmos. Environ.,* **31,** 73–80.

Pinsky, M., A. Khain, and M. Shapiro, 1999: Collisions of small

drops in a turbulent flow. Part I: Collision efficiency. Problem formulation and preliminary results. *J. Atmos. Sci.*, **56,** 2585–2600.

——, ——, and ——, 2000: Stochastic effects of cloud droplet hydrodynamic interaction in a turbulent flow. *Atmos. Res.*, **53,** 131–169.

——, ——, and ——, 2001: Collision efficiency of drops in a wide range of Reynolds numbers: Effects of pressure on spectrum evolution. *J. Atmos. Sci.*, **58,** 742–764.

Rogers, R. R., and M. K. Yau, 1989: *A Short Course in Cloud Physics.* 3d ed. Pergamon Press, 293 pp.

Rosenfeld, D., 1999: TRMM observed first direct evidence of smoke from forest fires inhibiting rainfall. *Geophys. Res. Lett.*, **26,** 3105–3108.

Squires, P., 1958: The microstructure and colloidal stability of warm clouds. *Tellus*, **10,** 256–261.

Szumowski, M. J., R. M. Rauber, and H. T. Ochs III, 1999: The microphysical structure and evolution of Hawaiian rainband clouds. Part III: A test of the ultragiant nuclei hypothesis. *J. Atmos. Sci.*, **56,** 1980–2003.

Woodcock, A. H., 1953: Salt nuclei in maritime air as a function of altitude and wind force. *J. Meteor.*, **10,** 362–371.